Hermite interpolation by piecewise polynomial surfaces with rational offsets

B. Jüttler[a,*] M.L. Sampoli[b]

[a] *Dept. of Mathematics, University of Technology, Darmstadt, Germany*
[b] *Department of Mathematics, University of Siena, Siena, Italy*

Formatted November 28, 2003

Abstract

We present a construction for polynomial spline surfaces with a piecewise linear field of normal vectors. As main advantageous feature these surfaces possess exact rational offsets. The spline surface is composed of quartic Clough–Tocher–type macro elements. Each element is capable of matching boundary data consisting of three points with associated normal vectors. The collection of the macro elements forms a G^1 continuous spline surface. With the help of a reparamaterization technique we obtain an exact rational representation of the offset surfaces by rational triangular spline surfaces of degree 10.

Keywords: rational offset surfaces, Clough–Tocher split, Hermite interpolation.

1 Introduction

Offsets to curves and surfaces are required in various applications, such as milling and layered manufacturing. Currently, most CAD systems rely on approximation techniques for describing offsets. A comparative survey of approximation schemes for offsets to planar curves has been given recently by Elber, Lee and Kim (1997). Methods for approximating offset surfaces have been discussed by Barnhill and Frost (1995), Elber and Cohen (1991), Farouki (1986), Hoschek and Schneider (1989) and Patrikalakis and Prakash (1987).

*E-mail: juettler@mathematik.tu-darmstadt.de

Another approach to offsetting is that of considering only rational curves and surfaces with truly rational offsets, making it possible to represent both a certain shape and its offsets *exactly* within a CAD system. A suitable class of planar curves, the so-called Pythagorean hodograph (PH) curves, has been identified by Farouki (1994). These curves form a sub–class of integral Bézier curves; they are distinguished by having a first derivative vector (hodograph) the components of which belong to a Pythagorean triple. Consequently, PH curves have exactly rational offset curves and a polynomial arc length function. With the help of complex calculus, several constructions for PH spline curves from various input data has been developed, see e.g. (Farouki and Neff, 1995) and the references cited therein.

Based on the dual representation of planar curves, Pottmann (1995), and independently Fiorot and Gensane (1994), have derived an elegant construction of rational PH curves, see also (Farouki and Pottmann, 1996). Following the dual approach, a curve is generated as the envelope of its tangent lines. This construction can be generalized to surfaces, leading to the class of rational PN (Pythagorean normal) surfaces (Pottmann, 1995). As an application of this geometric approach, and with the help of concepts from Laguerre geometry, Peternell and Pottmann (1996) have designed PN surfaces by composing segments of parabolic Dupin cyclides , see also (Peternell, 1997).

The dual approach to surfaces with rational offsets can be traced back to a report by Sabin (1974), which also provides some earlier references on the representation of offset surfaces in CAD.

Working with the dual representation is an elegant geometrical idea, and it provides a very general construction of the available rational surfaces. However, as already observed by Sabin (1974), designing a surface by its dual representation (i.e. via the system of its tangent planes) is not very intuitive, and it may be difficult to avoid singularities and points at infinity.

In the conference article (Jüttler, 1998), triangular Bézier surface patches with a linear field of normal vectors (the so–called LN surface patches) have been shown to possess rational offset surfaces. This fact generalizes the rational offset property of parabolas to the surface case, see (Farouki and Sederberg, 1995). Using LN surfaces it is possible to circumvent the problems that are caused by the dual representation.

The present paper describes an interpolation scheme that generates LN spline surfaces from G^1 Hermite point data (data points with associated normal vectors). The LN spline surface is composed of Clough–Tocher–type macro elements interpolating three vertices and associated normal vectors. The individual macro elements are obtained from a local construction, only based on the geometric information at the vertices. The construction of the LN spline surface is suitable for converting a given surface (which is assumed to have no parabolic points) approximately into LN

spline form, by sampling sufficiently dense data. We discuss the existence and the regularity of the approximations generated by the Hermite interpolation scheme.

In order to find the rational representation of the offsets, we construct a suitable rational reparameterization that transforms the linear field of normal vectors into another field satisfying a Pythagorean condition. After applying this substitution, we obtain an exact rational representation of the offset surfaces, as rational triangular Bézier patches of degree 10.

2 Surfaces with linear normals

Recall that a triangular Bézier surface patch of degree n is defined by the parametric representation

$$\mathbf{x}(r,s,t) = \sum_{\substack{i,j,k \geq 0 \\ i+j+k=n}} \mathbf{b}_{i,j,k}\, B^n_{i,j,k}(r,s,t) \qquad r,s,t \geq 0, \quad r+s+t = 1, \tag{1}$$

with the control points $\mathbf{b}_{i,j,k} \in \mathbb{R}^3$. The blending functions are the bivariate Bernstein polynomials $B^n_{i,j,k}(r,s,t) = \frac{n!}{i!j!k!}\, r^i\, s^j\, t^k$. The domain of the patch is a triangle $\triangle \subset \mathbb{R}^2$; its points are represented by the barycentric parameters r, s, t. For additional information the reader should consult (Farin, 1986) or any textbook on Computer Aided Geometric Design, e.g. (Hoschek and Lasser, 1993).

Consider the first directional derivatives whose directions are parallel to the edges of the domain triangle $\triangle$. They can be expressed in Bézier form as

$$\begin{aligned}
\mathbf{x}_1(r,s,t) &= \frac{\mathrm{d}}{\mathrm{d}u}\mathbf{x}(r, s-u, t+u)\Big|_{u=0} = n \sum_{\substack{i,j,k \geq 0 \\ i+j+k=n-1}} \Delta_1\mathbf{b}_{i,j,k}\, B^{n-1}_{i,j,k}(r,s,t), \\
\mathbf{x}_2(r,s,t) &= \frac{\mathrm{d}}{\mathrm{d}u}\mathbf{x}(r+u, s, t-u)\Big|_{u=0} = n \sum_{\substack{i,j,k \geq 0 \\ i+j+k=n-1}} \Delta_2\mathbf{b}_{i,j,k}\, B^{n-1}_{i,j,k}(r,s,t), \\
\mathbf{x}_3(r,s,t) &= \frac{\mathrm{d}}{\mathrm{d}u}\mathbf{x}(r-u, r+u, r)\Big|_{u=0} = n \sum_{\substack{i,j,k \geq 0 \\ i+j+k=n-1}} \Delta_3\mathbf{b}_{i,j,k}\, B^{n-1}_{i,j,k}(r,s,t),
\end{aligned} \tag{2}$$

with the coefficients

$$\begin{gathered}
\Delta_1\mathbf{b}_{i,j,k} = \mathbf{b}_{i,j,k+1} - \mathbf{b}_{i,j+1,k}, \qquad \Delta_2\mathbf{b}_{i,j,k} = \mathbf{b}_{i+1,j,k} - \mathbf{b}_{i,j,k+1}, \\
\text{and} \quad \Delta_3\mathbf{b}_{i,j,k} = \mathbf{b}_{i,j+1,k} - \mathbf{b}_{i+1,j,k}.
\end{gathered} \tag{3}$$

The field of normal vectors $\vec{\mathbf{N}}(r,s,t) \not\equiv \vec{\mathbf{0}}$ of the Bézier patch (1) fulfills the equations

$$\mathbf{x}_l(r,s,t) \cdot \vec{\mathbf{N}}(r,s,t) \equiv 0, \quad \text{for} \quad l = 1,2,3, \tag{4}$$

with the standard inner product '$\cdot$'. Note that any two of the three equations imply the third one, as the first directional derivatives satisfy

$$\mathbf{x}_1(r,s,t) + \mathbf{x}_2(r,s,t) + \mathbf{x}_3(r,s,t) = 0. \tag{5}$$

Clearly, a possible field of normal vectors can be obtained as the cross product of any two directional derivatives, e.g.

$$\vec{\mathbf{N}}^*(r,s,t) = \mathbf{x}_1(r,s,t) \times \mathbf{x}_2(r,s,t). \tag{6}$$

Generally, this leads to a bivariate polynomial of degree $2n-2$. In the sequel we concentrate our attention on Bézier patches whose normal vectors have the lowest possible degree.

Definition 1 *The triangular Bézier surface patch (1) is said to be a surface with a linear field of normal vectors ('LN patch' for short), if it has normal vectors of the form*

$$\begin{aligned} \vec{\mathbf{N}}(r,s,t) &= r\,\vec{\mathbf{n}}_1 + s\,\vec{\mathbf{n}}_2 + t\,\vec{\mathbf{n}}_3 \\ &= B^1_{1,0,0}(r,s,t)\,\vec{\mathbf{n}}_1 + B^1_{0,1,0}(r,s,t)\,\vec{\mathbf{n}}_2 + B^1_{0,0,1}(r,s,t)\,\vec{\mathbf{n}}_3 \end{aligned} \tag{7}$$

with certain coefficients (called the vertex normals) $\vec{\mathbf{n}}_i \in \mathbb{R}^3$.

If the surface patch (1) is an LN patch, then the normal vectors $\vec{\mathbf{N}}^*$ and $\vec{\mathbf{N}}$ (obtained from (6) and (7), respectively) are linearly dependent. Consequently,

$$\vec{\mathbf{N}}^*(r,s,t) = \lambda(r,s,t)\,\vec{\mathbf{N}}(r,s,t) \tag{8}$$

holds with some bivariate function $\lambda(r,s,t)$. If the vertex normals $\vec{\mathbf{n}}_i$ of $\vec{\mathbf{N}}(r,s,t)$ are linearly independent, then λ is guaranteed to be a bivariate polynomial. Thus, the LN patches among the Bézier surfaces (1) could be characterized by normal vectors (6) whose components share a polynomial factor λ of degree $2n-3$. This characterization, however, is not very useful. Instead, we obtain from (2) and (4) conditions for the control points of LN surfaces.

Lemma 2 *The surface patch* $\mathbf{x}(r,s,t)$ *is an LN patch with the normal vectors (7), if and only if its control points satisfy the equations*

$$\frac{i}{n}\vec{\mathbf{n}}_1 \cdot \Delta_l \mathbf{b}_{i-1,j,k} + \frac{j}{n}\vec{\mathbf{n}}_2 \cdot \Delta_l \mathbf{b}_{i,j-1,k} + \frac{k}{n}\vec{\mathbf{n}}_3 \cdot \Delta_l \mathbf{b}_{i,j,k-1} = 0 \quad i,j,k \geq 0,\ \ i+j+k = n, \tag{9}$$

for any two values of $l \in \{1,2,3\}$, *where* $\Delta_l \mathbf{b}_{i,j,k} = 0$ *whenever* $\min\{i,j,k\} < 0$. *If the vertex normals* $\vec{\mathbf{n}}_i$ *are given, then we obtain from (9) a system of* $2\binom{n+2}{2}$ *linear equations for the* $3\binom{n+2}{2}$ *components of the control points* $\mathbf{b}_{i,j,k}$.

The offset (or parallel) surface to the patch $\mathbf{x}(r,s,t)$ at a certain distance $d \in \mathbb{R}$ has the representation

$$\mathbf{x}_d(r,s,t) = \mathbf{x}(r,s,t) + \frac{d}{\|\vec{\mathbf{N}}(r,s,t)\|}\,\vec{\mathbf{N}}(r,s,t), \tag{10}$$

with $\|\vec{\mathbf{N}}(r,s,t)\| = \sqrt{\vec{\mathbf{N}}(r,s,t)\cdot\vec{\mathbf{N}}(r,s,t)}$. Generally, the offset is not a rational surface, due to the square root in the denominator of (10). As an advantageous feature, LN patches have rational offsets:

Theorem 3 *The offset surfaces of LN patches can be represented exactly as rational triangular Bézier surfaces.*

This result has been derived in (Jüttler, 1998), by generalizing the rational offset property of parabolas to the surface case. The details of the proof will be presented in Section 5, along with a construction of the rational Bézier patches that describe the offsets of the LN surface. This construction is based on a reparameterization technique that transforms the linear normal vector field in another field satisfying a Pythagorean condition.

3 Compatibility conditions

LN surface patches are characterized by (4) and (7). These conditions entail certain technical compatibility conditions which need to be taken into account of when developing a scheme for the construction of LN spline surfaces interpolating given data.

Lemma 4 *The control points $\mathbf{b}_{i,j,k}$ of an LN patch with the normal vectors (7) satisfy the following compatibility conditions:*

(*i*) *Compatibility at the vertex $\mathbf{x}(0,0,1)$ of the patch (cf. Figure 1a),*

$$(\vec{\mathbf{n}}_3 - \vec{\mathbf{n}}_1)\cdot(\mathbf{b}_{0,1,n-1} - \mathbf{b}_{0,0,n}) = (\vec{\mathbf{n}}_3 - \vec{\mathbf{n}}_2)\cdot(\mathbf{b}_{1,0,n-1} - \mathbf{b}_{0,0,n}). \tag{11}$$

(*ii*) *Compatibility along a boundary curve,*

$$(\Delta_3)^n\,\mathbf{b}_{0,0,0}\cdot(\vec{\mathbf{n}}_3 - \vec{\mathbf{n}}_1) = (\Delta_3)^n\,\mathbf{b}_{0,0,0}\cdot(\vec{\mathbf{n}}_3 - \vec{\mathbf{n}}_2) = 0, \tag{12}$$

where the n–th difference vector $(\Delta_3)^n\,\mathbf{b}_{0,0,0}$ involves only the control points along the boundary $\mathbf{x}(1-u,u,0)$, cf. Figure 1b.

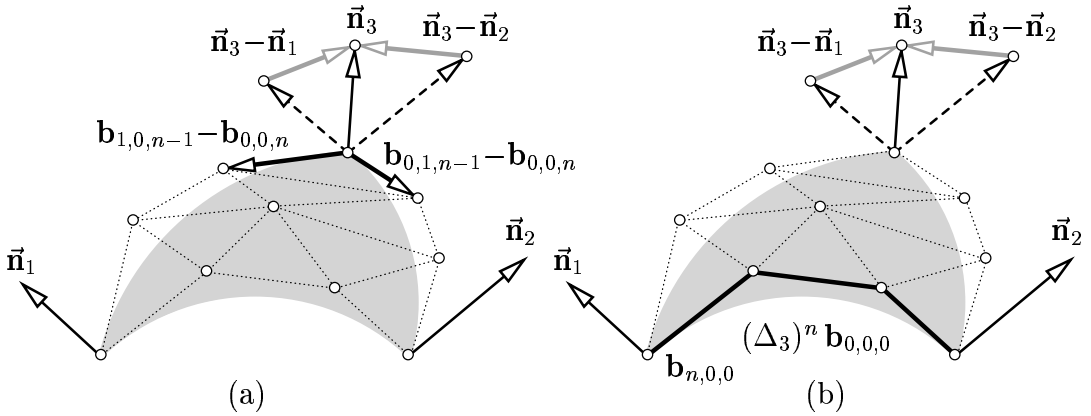

Figure 1: Compatibility conditions for LN patches (scheme).

Proof. Differentiating the identities $\vec{\mathbf{N}} \cdot \mathbf{x}_2 = \vec{\mathbf{N}} \cdot \mathbf{x}_1 = 0$ in the directions that are parallel to the first resp. second edge of the domain triangle we obtain

$$\vec{\mathbf{N}}_1 \cdot \mathbf{x}_2 + \vec{\mathbf{N}} \cdot \mathbf{x}_{12} = \vec{\mathbf{N}}_2 \cdot \mathbf{x}_1 + \vec{\mathbf{N}} \cdot \mathbf{x}_{12}, \quad \text{hence} \quad \vec{\mathbf{N}}_1 \cdot \mathbf{x}_2 = \vec{\mathbf{N}}_2 \cdot \mathbf{x}_1. \tag{13}$$

Here, the (multi–) index denotes the (iterated) directional differentiation of the patch $\mathbf{x}(r,s,t)$ and the associated linear normal vectors (7), cf. (2). In particular,

$$\vec{\mathbf{N}}_1 = \vec{\mathbf{n}}_3 - \vec{\mathbf{n}}_2, \quad \vec{\mathbf{N}}_2 = \vec{\mathbf{n}}_1 - \vec{\mathbf{n}}_3, \quad \vec{\mathbf{N}}_3 = \vec{\mathbf{n}}_2 - \vec{\mathbf{n}}_1. \tag{14}$$

Evaluating (13) at $(r,s,t) = (0,0,1)$ gives (11).

In order to prove the remaining condition, we differentiate the identity $\vec{\mathbf{N}} \cdot \mathbf{x}_1 = 0$ from (4) n times with respect to the third direction. Note that the second order derivatives of $\vec{\mathbf{N}}(r,s,t)$ vanish. With the help of these observations we arrive at

$$n\,\vec{\mathbf{N}}_3 \cdot \mathbf{x}_{1\underbrace{33\ldots3}_{n-1 \text{ times}}} + \vec{\mathbf{N}} \cdot \mathbf{x}_{1\underbrace{33\ldots3}_{n \text{ times}}} = 0, \quad \text{hence} \quad \vec{\mathbf{N}}_3 \cdot \mathbf{x}_{1\underbrace{33\ldots3}_{n-1 \text{ times}}} = 0, \tag{15}$$

as the $(n{+}1)$st order derivatives of $\mathbf{x}(r,s,t)$ vanish as well. Similarly, differentiating $\vec{\mathbf{N}} \cdot \mathbf{x}_3 = 0$ once with respect to the first direction and $(n{-}1)$ times with respect to the third direction one gets

$$\vec{\mathbf{N}}_1 \cdot \mathbf{x}_{\underbrace{33\ldots3}_{n \text{ times}}} + (n-1)\,\vec{\mathbf{N}}_3 \cdot \mathbf{x}_{1\underbrace{33\ldots3}_{n-1 \text{ times}}}. \tag{16}$$

According to (15), the second term vanishes. Using (2) and (14) we obtain

$$(\vec{\mathbf{n}}_3 - \vec{\mathbf{n}}_2) \cdot (\Delta_3)^n\,\mathbf{b}_{0,0,0} = 0. \tag{17}$$

Finally, applying n–fold directional differentiation to $\vec{\mathbf{N}} \cdot \mathbf{x}_3$ gives

$$\vec{\mathbf{N}}_3 \cdot \mathbf{x}_{\underbrace{33\ldots3}_{n \text{ times}}} = (\vec{\mathbf{n}}_2 - \vec{\mathbf{n}}_1) \cdot (\Delta_3)^n\,\mathbf{b}_{0,0,0} = 0. \tag{18}$$

Combining this observation with (17) completes the proof of (12). □

Clearly, analogous conditions are satisfied at the remaining vertices and boundaries of an LN patch. From these compatibility conditions we draw the following consequences regarding possible constructions of LN spline surface from given data.

1. In order to construct two boundaries of an LN patch independently of each other, we would have to use singular vertices, i.e. coinciding corner control points $\mathbf{b}_{0,1,n-1} = \mathbf{b}_{0,0,n} = \mathbf{b}_{1,0,n-1}$. Otherwise, the control points of the boundaries are coupled by condition (11).

2. In order to design a boundary of an LN patch independently of the normal vector at the opposite vertex, we have to use a curve of reduced degree $n-1$. Consequently, the compatibility condition (12) is trivially satisfied with $(\Delta_l)^n \mathbf{b}_{0,0,0} = \vec{\mathbf{0}}$. Otherwise the boundary curve and the normal vector at the opposite vertex are coupled by condition (12).

4 Hermite interpolation with LN macro elements

We consider the following Hermite interpolation problem. Given three points (vertices) $\mathbf{v}_i \in \mathbb{R}^3$ with associated normal vectors $\vec{\mathbf{m}}_i \in \mathbb{R}^3$ $(i = 1, 2, 3)$, find a piecewise LN surface patch that interpolates these data. Here, we will concentrate on the interpolation of only three data, leading to a *triangular LN macro element*. Later, several elements will be put together in order to construct LN spline surfaces.

A similar macro element has been presented by the first author in (Jüttler, 1998). However, that construction was based on singularly parameterized vertices, in order to satisfy the compatibility condition (i) of Lemma 4. Moreover, the degree of the patches is relatively high (six), which may entail difficulties with the parameterization of the offsets.

The aim of this paper is to present an improved construction, providing the following features.

1. *Locality.* The construction of the macro elements is to proceed locally, as far as possible. For instance, both the boundary curve connecting the points $\mathbf{v}_1$, $\mathbf{v}_2$ and the normals along this boundary should depend solely on these vertices and on the associated normals $\vec{\mathbf{m}}_1$, $\vec{\mathbf{m}}_2$, but not on the data $\mathbf{v}_3$, $\vec{\mathbf{m}}_3$ at the opposite vertex. Consequently, the macro elements will be suitable for building G^1 spline surfaces, as macro elements sharing two boundary data will automatically meet with G^1 continuity.

2. *Regularity.* The resulting triangular Bézier patches are expected to be regular. That is, any two of the first directional derivatives (2) should be linearly indepen-

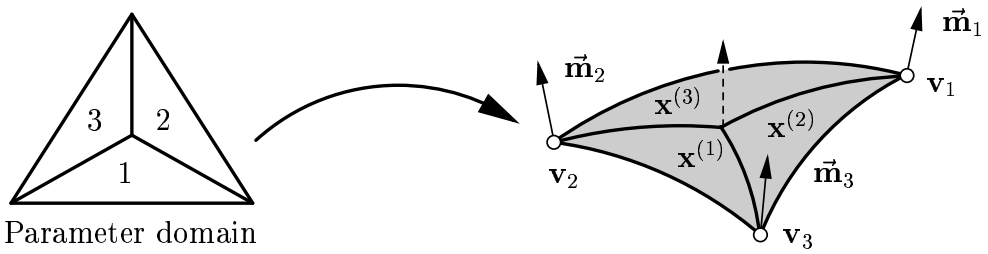

Figure 2: Clough–Tocher–type macro element and the given data.

dent at all points, thus leading to a well–defined tangent plane everywhere. Using a suitable type of macro elements we are able to avoid singularly parameterized vertices (cf. the compatibility condition Lemma 4(i) and its consequence). Clearly, the regularity of the resulting surface depends on the input data also. We present some results concerning the regularity of the patches for data that are taken from surfaces without parabolic points.

3. *Minimum degree.* The polynomial degree of the triangular Bézier patches should be as low as possible. This is important, as the rational representation of the offset surfaces are found with the help of a quadratic rational reparameterization that leads to a higher polynomial degree. Thus, it is advantageous to start from a relatively low degree. We show that the minimum possible degree is four and interpolate the data with quartic macro elements.

4.1 Clough–Tocher–type macro elements

We interpolate the three data $(\mathbf{v}_i, \vec{\mathbf{m}}_i)$ by three LN patches, forming a Clough–Tocher–type macro element, see Figure 2, cf. (Hoschek and Lasser, 1993, p.411), or (Clough and Tocher, 1965).

The l–th patch $\mathbf{x}^{(l)}(r,s,t)$ has the parametric representation (1) with control points $\mathbf{b}^{(l)}_{i,j,k} \in \mathbb{R}^3$, $l \in \{1,2,3\}$. Its linear normal field is given by (7), with the coefficient vectors $\vec{\mathbf{n}}^{(l)}_i$,

$$\begin{gathered}\vec{\mathbf{n}}^{(1)}_1 = \vec{\mathbf{n}}^{(3)}_2 = \vec{\mathbf{m}}_2, \quad \vec{\mathbf{n}}^{(2)}_1 = \vec{\mathbf{n}}^{(1)}_2 = \vec{\mathbf{m}}_3, \quad \vec{\mathbf{n}}^{(3)}_1 = \vec{\mathbf{n}}^{(2)}_2 = \vec{\mathbf{m}}_1, \\ \text{and} \quad \vec{\mathbf{n}}^{(1)}_3 = \vec{\mathbf{n}}^{(2)}_2 = \vec{\mathbf{n}}^{(3)}_3 = \tfrac{1}{3}(\vec{\mathbf{m}}_1 + \vec{\mathbf{m}}_2 + \vec{\mathbf{m}}_3).\end{gathered} \tag{19}$$

Here, the normal vector at the interior vertex of the Clough–Tocher split (shown as the dashed vector in Figure 2) is simply chosen as the average of the boundary normals $\vec{\mathbf{m}}_i$. In consequence of (7), the control points $\mathbf{b}^{(l)}_{i,j,k}$ of the three patches satisfy certain linear equations (9), according to Lemma 2.

The three patches are to interpolate the given vertices,

$$\begin{gathered}\mathbf{v}_1 = \mathbf{x}^{(2)}(0,1,0) = \mathbf{x}^{(3)}(1,0,0), \quad \mathbf{v}_2 = \mathbf{x}^{(3)}(0,1,0) = \mathbf{x}^{(1)}(1,0,0), \\ \text{and} \quad \mathbf{v}_3 = \mathbf{x}^{(1)}(0,1,0) = \mathbf{x}^{(2)}(1,0,0).\end{gathered} \tag{20}$$

This entails the conditions

$$\mathbf{v}_1 = \mathbf{b}^{(2)}_{0,n,0} = \mathbf{b}^{(3)}_{n,0,0}, \quad \mathbf{v}_2 = \mathbf{b}^{(3)}_{0,n,0} = \mathbf{b}^{(1)}_{n,0,0}, \quad \text{and} \quad \mathbf{v}_3 = \mathbf{b}^{(1)}_{0,n,0} = \mathbf{b}^{(2)}_{n,0,0}. \tag{21}$$

Finally, the three LN patches are required to meet continuously along the inner boundaries of the macro element, i.e.

$$\begin{gathered}\mathbf{x}^{(1)}(0,1{-}u,u) = \mathbf{x}^{(2)}(1{-}u,0,u), \quad \mathbf{x}^{(2)}(0,1{-}u,u) = \mathbf{x}^{(3)}(1{-}u,0,u), \\ \text{and} \quad \mathbf{x}^{(3)}(0,1{-}u,u) = \mathbf{x}^{(1)}(1{-}u,0,u),\end{gathered} \tag{22}$$

or, equivalently,

$$\mathbf{b}^{(1)}_{0,i,j} = \mathbf{b}^{(2)}_{i,0,j}, \quad \mathbf{b}^{(2)}_{0,i,j} = \mathbf{b}^{(3)}_{i,0,j}, \quad \text{and} \quad \mathbf{b}^{(3)}_{0,i,j} = \mathbf{b}^{(1)}_{i,0,j} \quad (i,j \in \mathbb{Z}_+,\ i+j=n). \tag{23}$$

Note that, in addition to (22), the normal vectors of the three LN patches are identical along the inner boundaries, see (7) and (19). Thus, the macro element is even G^1 continuous.

4.2 Boundary curves

First we construct the boundary curves of the macro element. For instance, consider the boundary curve $\mathbf{y}(u) = \mathbf{x}^{(3)}(1{-}u,u,0)$, running from $\mathbf{v}_1$ to $\mathbf{v}_2$, with the associated normals $\vec{\mathbf{m}}_1$, $\vec{\mathbf{m}}_2$. The boundary is chosen as a cubic Bézier curve

$$\mathbf{y}(u) = \mathbf{v}_1\, B^3_0(u) + \mathbf{p}_1\, B^3_1(u) + \mathbf{p}_2\, B^3_2(u) + \mathbf{v}_2\, B^3_3(u), \quad u \in [0,1], \tag{24}$$

with the univariate Bernstein polynomials $B^n_i(u)$. The inner control points $\mathbf{p}_1$, $\mathbf{p}_2$ are unknown. Clearly, the LN conditions (4) have to be satisfied along the boundary, i.e.,

$$0 = \mathbf{x}^{(3)}_3(u,1-u,0) \cdot \vec{\mathbf{N}}^{(3)}(u,1-u,0) = [\, \frac{\mathrm{d}}{\mathrm{d}u}\mathbf{y}(u)\,] \cdot [\,(1{-}u)\,\mathbf{m}_1 + u\,\mathbf{m}_2\,], \tag{25}$$

with the linear normal vector $\vec{\mathbf{N}}^{(3)}$ of the patch $\mathbf{x}^{(3)}$, see (7) and (19). This leads to the 4 linear equations

$$\begin{gathered}(\mathbf{p}_1 - \mathbf{v}_1)\cdot\vec{\mathbf{m}}_1 = 0, \quad 2\,(\mathbf{p}_2 - \mathbf{p}_1)\cdot\vec{\mathbf{m}}_1 + (\mathbf{p}_1 - \mathbf{v}_1)\cdot\vec{\mathbf{m}}_2 = 0, \\ (\mathbf{v}_2 - \mathbf{p}_2)\cdot\vec{\mathbf{m}}_1 + 2\,(\mathbf{p}_2 - \mathbf{p}_1)\cdot\vec{\mathbf{m}}_2 = 0, \quad (\mathbf{v}_2 - \mathbf{p}_2)\cdot\vec{\mathbf{m}}_2 = 0\end{gathered} \tag{26}$$

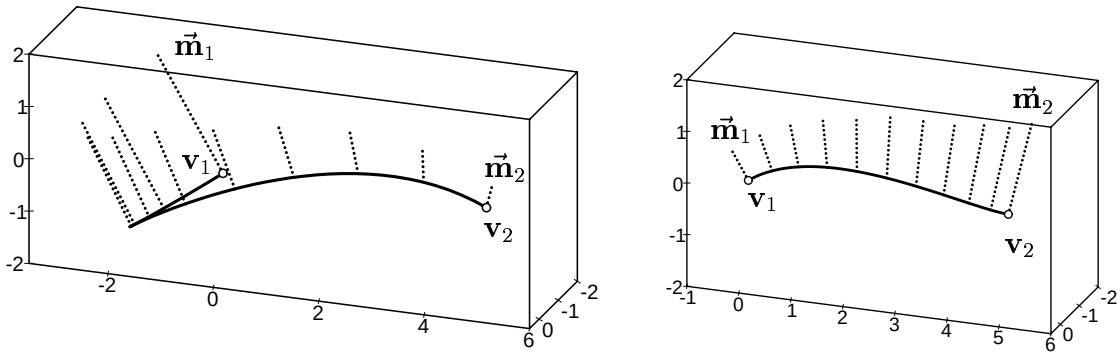

Figure 3: Boundary curves of LN patches

for the 6 components of the unknown control points $\mathbf{p}_1$, $\mathbf{p}_2$. We pick the solution that minimizes the squared length of the control polygon,

$$F(\mathbf{p}_1, \mathbf{p}_2) = \|\mathbf{p}_1 - \mathbf{v}_1\|^2 + \|\mathbf{p}_2 - \mathbf{p}_1\|^2 + \|\mathbf{v}_2 - \mathbf{p}_2\|^2, \tag{27}$$

hence generating a special minimum norm network of boundary curves, cf. (Kolb, Pottmann and Seidel, 1995) and the references cited therein. The solution of the constrained quadratic optimization problem $F \to \text{Min.}$, subject to (26), can be computed by solving a linear system, using Lagrangian multipliers.

Lemma 5 *The quadratic optimization problem $F \to$ Min., subject to (26), has a unique solution if and only if the normal vectors $\vec{\mathbf{m}}_1$ and $\vec{\mathbf{m}}_2$ are linearly independent.*

Proof. The Lagrangian multiplier technique leads to a 10×10 linear system. The determinant of its coefficient matrix factors into $108\,\|\vec{\mathbf{m}}_1 \times \vec{\mathbf{m}}_2\|^4$. This proves the assertion. □

Clearly, if the normal vectors $\vec{\mathbf{m}}_1$ and $\vec{\mathbf{m}}_2$ are linearly dependent, then the boundary curve has to be contained in a plane perpendicular to both $\vec{\mathbf{m}}_1$ and $\vec{\mathbf{m}}_2$. Hence, in this case solutions can exist only if the difference vector $\mathbf{v}_2 - \mathbf{v}_1$ is perpendicular to both $\vec{\mathbf{m}}_1$ and $\vec{\mathbf{m}}_2$.

Two examples of boundary curves are shown in Figure 3. Both curves interpolate the same boundary points $\mathbf{v}_1$, $\mathbf{v}_2$. The associated boundary normals $\vec{\mathbf{m}}_1$ and $\vec{\mathbf{m}}_2$ have identical directions, but different lengths. This leads to a different distribution of the normals along the boundary (shown as the dotted lines), hence to different boundary curves. The left curve has an undesired loop, while the right curve behaves as expected. In the next theorem we discuss the shape of the solutions for data which are taken from a smooth surface without parabolic points (i.e., Gaussian curvature $K \neq 0$ everywhere).

Theorem 6 *Let Φ be a C^3 surface patch which is assumed to have no parabolic points, i.e. non–zero Gaussian curvature. Consider two points $\mathbf{v}_1$, $\mathbf{v}_2$ on Φ with associated unit normals $\vec{\mathbf{m}}_1$, $\vec{\mathbf{m}}_2$, i.e. $\|\vec{\mathbf{m}}_i\| = 1$. Applying the construction of Lemma 5 to these data produces a cubic boundary curve $\mathbf{y}(t)$, see (24). The following assertions are true, provided that the distance (stepsize) between the points $\mathbf{v}_1$, $\mathbf{v}_2$ is sufficiently small.*

(*i*) *The problem $F \to Min.$, subject to (26), has a unique solution.*

(*ii*) *The solution exhibits the desired shape, running directly from $\mathbf{v}_1$ to $\mathbf{v}_2$ without loops or cusps. More precisely, consider the straight line segment*

$$(1-u)\,\mathbf{v}_1 + u\,\mathbf{v}_2, \quad u \in [0,1].$$

For decreasing stepsize, the cubic boundary $\mathbf{y}(u)$ matches the shape and the parameterization of this line segment.

Proof. Without loss of generality we may choose $\mathbf{v}_1 = (0,0,0)^\top$ and $\vec{\mathbf{n}}_1 = (0,0,1)^\top$. Then, in a neighbourhood of $\mathbf{v}_1$, the surface can be approximated by the graph $(x, y, F(x,y))^\top$ of the bivariate Taylor series

$$\begin{array}{rcl} F(x,y) & = & \frac{1}{2} f_{11}\, x^2 + f_{12}\, x\, y + \frac{1}{2} f_{22}\, y^2 \\ & + & \frac{1}{6} f_{111}\, x^3 + \frac{1}{2} f_{112}\, x^2\, y + \frac{1}{2} f_{122}\, x\, y^2 + \frac{1}{6} f_{222}\, y^3 + \ldots \end{array} \tag{28}$$

with certain coefficients $f, f_i, f_{ij}, \ldots$. The indices $1, 2$ of f refer to the partial derivatives respect to x and y at the origin $(x,y) = (0,0)$. Owing to the choice of $\mathbf{v}_1$, $\mathbf{n}_1$ we get $0 = f = f_1 = f_2$. The second point $\mathbf{v}_2$ is chosen with its abscissas $(h, 0)$ on the x–axis, with the stepsize $h > 0$.

$$\mathbf{v}_2 = (h,\ \ 0,\ \ \tfrac{1}{2} f_{11}\, h^2 + \tfrac{1}{6} f_{111}\, h^3 + \ldots)^\top. \tag{29}$$

The associated normal vector $\vec{\mathbf{m}}_2$ is obtained by normalizing the cross product of the partial derivatives of $(x, y, F(x,y))$ at $(x,y) = (h,0)$. This leads to the Taylor expansion

$$\vec{\mathbf{m}}_2 = \begin{pmatrix} -f_{11}h - \frac{1}{2} f_{111} h^2 + \left(-\frac{1}{6} f_{1111} + \frac{1}{2} {f_{11}}^3 + \frac{1}{2} f_{11} {f_{12}}^2\right) h^3 + \ldots \\ -f_{12}h - \frac{1}{2} f_{112} h^2 + \left(-\frac{1}{6} f_{1112} + \frac{1}{2} f_{12} {f_{11}}^2 + \frac{1}{2} {f_{12}}^3\right) h^3 + \ldots \\ 1 + \left(-\frac{1}{2} {f_{11}}^2 - \frac{1}{2} {f_{12}}^2\right) h^2 + \left(-\frac{1}{2} f_{11} f_{111} - \frac{1}{2} f_{12} f_{112}\right) h^3 + \ldots \end{pmatrix}. \tag{30}$$

Combining this result with $\vec{\mathbf{m}}_1 = (0,0,1)^\top$ we get

$$\|\vec{\mathbf{m}}_1 \times \vec{\mathbf{m}}_2\|^2 = \left({f_{11}}^2 + {f_{12}}^2\right)\ h^2 + \left(f_{12} f_{112} + f_{11} f_{111}\right)\ h^3 + \ldots. \tag{31}$$

If $(f_{11}, f_{12}) \neq (0,0)$ and the stepsize h is sufficiently small, then a unique interpolating boundary curve exists, cf. Lemma 5. The first condition is violated if and only if $\vec{\mathbf{v}}_1$ is

a parabolic point of the surface with the asymptotic direction $(0,1,0)^\top$. This proves the first part (i) of the theorem.

Using suitable computer algebra tools such as Maple or Mathematica, the problem $F \to \text{Min.}$, subject to (26), is solved for the Taylor expansions of the data $\mathbf{v}_i$ with associated unit normals $\vec{\mathbf{m}}_i$. This produces an expansion of the boundary curve

$$\mathbf{y}(u) = \begin{pmatrix} u\,h + (u\,(1-u)\,f_{11}f_{111}) \,/\, \left(2\,{f_{11}}^2 + 2\,{f_{12}}^2\right)\,h^2 + \ldots \\ (u\,(1-u)\,f_{12}f_{111}) \,/\, \left(2\,{f_{11}}^2 + 2\,{f_{12}}^2\right)\,h^2 + \ldots \\ \frac{1}{2}\,u^2 f_{11}\,h^2 + \ldots \end{pmatrix} \tag{32}$$

By comparing this Taylor series with that of the line segment $(1-u)\,\mathbf{v}_1 + u\,\mathbf{v}_2$, it can be seen that the difference between the two curves is in the order of $O(h^2)$. Consequently, the boundary curve (32) has the desired shape for sufficiently small h, without loops or cusps. This completes the proof. □

The theorem can now be applied to a triangulated cloud of data.

Corollary 7 *Consider a triangulated cloud of data with associated unit normals, both taken from a C^3 surface Φ without parabolic points, i.e. with non–zero Gaussian curvature. Assume that the collected facets of triangulation (i.e. the triangular mesh) reproduce the shape of the surface.*

For each edge of the triangulation, the above–described construction is used in order to find a cubic boundary curve. Then, provided that one has sampled sufficiently many and sufficiently dense data from the original surface (cf. Remark 1), all these boundary curves exist and are regular. Moreover, the facets of the resulting network of boundary curves match the shape of the facets of the triangular mesh.

Remark 1. The assumption of 'sufficiently dense' data is concerned with the quality of the triangulation of the data points. The corollary refers to a sequence of triangular meshes that is obtained by taking more and more sample points from the original surface. For this sequence, the inner angles of the triangular elements are assumed to be bounded strictly away from zero. That is, the triangles should not become arbitrarily long and thin. Then, by constructing LN boundaries for these triangular meshes, the assumption becomes true for sufficiently many data.

Remark 2. Cubic boundary curves have the lowest possible degree, if the boundaries are to consist of only one segment. By splitting the boundaries into two segments, it is possible to use quadratic boundaries. In this case, however, one would need to use triangular elements that are more complicated than the Clough–Tocher split. Here, it seems to be the most natural choice to consider Powell–Sabin–type elements, see (Hoschek and Lasser, 1993, p.412). However, it turns out that the degrees of freedom provided by these elements (with quadratic boundaries and cubic patches, owing to

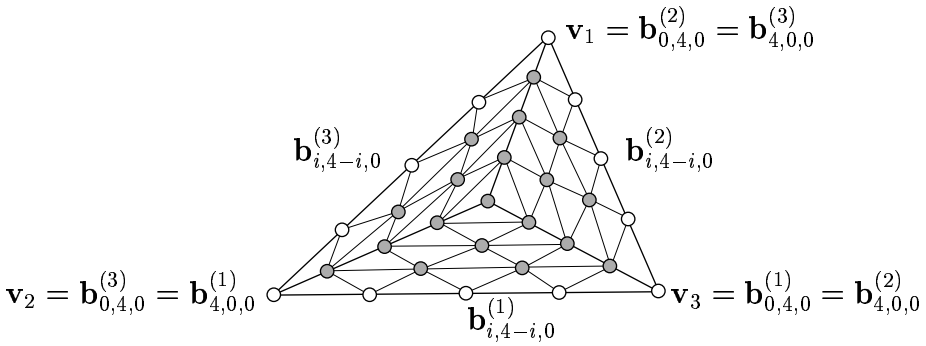

Figure 4: Free control points (grey dots) of the macro element.

the compatibility condition of Lemma 4) are not sufficient to match the three data $\mathbf{v}_i$ with associated normals $\vec{\mathbf{m}}_i$. Thus, more complicated splittings are required to obtain a minimum degree construction, and the increased number of sub–patches might well outweigh the advantages of the reduced degree. This may be a subject of further research.

4.3 Filling in the patches

In order to find the Clough–Tocher–type macro element that matches the three G^1 Hermite vertex data $(\mathbf{v}_i,\ \vec{\mathbf{m}}_i)$, we apply the construction of the previous section to the boundaries, cf. Figure 2. This produces three cubic boundary curves. According to the second compatibility condition (see Lemma 4), the interpolating macro element has to be composed of subpatches $\mathbf{x}^{(l)}(r,s,t)$, $l \in \{1,2,3\}$, of minimum degree $n = 4$. Raising the degrees of the boundaries by one gives the control points $\mathbf{b}^{(l)}_{i,4-i,0}$ along the exterior boundaries of the subpatches. Moreover, the control points along the inner boundaries are identical, cf. (23). Thus, after choosing the boundary curves we have 19 free control points, i.e. 57 degrees of freedom (cf. Figure 4).

Next we build up a system of equations that guarantee the desired linear field of normal vectors. By collecting the conditions obtained from (9) and (19) we obtain a system of $6\binom{6}{2} = 95$ equations. Some of these conditions, however, are redundant and can therefore be deleted from the system. For instance, the LN conditions are automatically satisfied along the edges of the macro element, due do the construction of the boundary curves. Further redundancies occur along the inner boundaries of the three subpatches. After eliminating the redundant equations we obtain a system of 54 equations for 57 unknowns. Unfortunately, we are not able to discuss the existence of solutions as in the case of the boundaries (cf. Lemma 5), as the current computer algebra systems fail to generate symbolic solutions. However, according to our numerical experiments, the system is solvable for data in general position.

As the 57 components of the unknown control points $\mathbf{b}^{(l)}_{i,j,k}$ have to satisfy only 54 equations, we have 3 degrees of freedom. A particular solution can be picked by

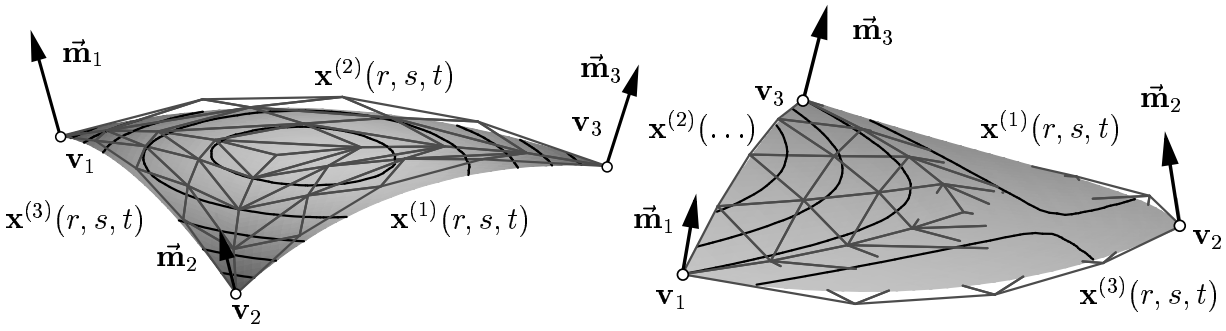

Figure 5: Clough–Tocher–type LN macro elements interpolating convex (left) and non–convex (right) data.

minimizing a suitable quadratic objective function, such as

$$G(b^{(l)}_{i,j,k}) = \sum_{\substack{l=1 \\ i+j+k=n-2}}^{3} \left((\Delta_1)^2 + (\Delta_2)^2 + (\Delta_2)^2 \right) \mathbf{b}^{(l)}_{ijk}, \quad i,j,k \geq 0. \tag{33}$$

This objective function is related to the squared second derivatives of the patches, hence it can be interpreted as some kind of fairness measure. (See Hoschek and Lasser (1993) for more information on fairness criteria for surfaces.) Similar to the construction of the boundaries, the solution of the constrained quadratic programming problem

$$G(\ldots) \to \text{Min.} \quad \text{subject to the LN conditions} \tag{34}$$

could be computed with the help of Lagrangian multipliers, leading to a quadratic system of equations with $57 + 54 = 111$ unknowns. Alternatively, one may compute the general solution of the underdetermined system of 54 equations which depends on 3 free parameters, and then pick the particular solution that minimizes (33).

Two examples are shown in Figure 5. For the first (resp. second) macro element, the data $(\mathbf{v}_i, \vec{\mathbf{m}}_i)$ have been taken from a convex (non–convex) surface. The resulting macro element is convex (resp. non–convex) also.

In addition to the surface patches, the figures show the Hermite boundary data $(\mathbf{v}_i, \vec{\mathbf{m}}_i)$ and the control nets $\{\mathbf{b}^{(l)}_{i,j,k}\}$ (thick grey lines) of the three sub–patches. Moreover we have drawn some intersection curves (solid lines) with parallel planes $z = \text{const.}$, in order to visualize the shape of the surfaces.

The shape of the boundary curves for data which are taken from a sufficiently smooth surface without parabolic points has been discussed in Theorem 6. So far we have not succeeded in deriving a similar result concerning the shape of the LN macro elements. However, we may state the following conjecture which is also supported by our numerical experiments.

Conjecture. *Consider a triangulated cloud of data with associated unit normals, both taken from a C^3 surface Φ without parabolic points, i.e. with non–zero Gaussian curvature. Assume that the collected facets of triangulation reproduce the shape of the surface. For each facet of the triangulation, we construct a LN macro element. Then, provided that one has sampled sufficiently many and sufficiently dense data (see Remark 1 after Corollary 7) from the original surface, all these macro elements exist and are regular, and they reproduce the shape of the original surface.*

Remark 1. LN patches are not capable of describing surfaces having both elliptic (i.e. locally convex) and hyperbolic points, as they have difficulties with representing parabolic points. Parabolic points correspond to *singular* points of the field of normal vectors. Those points are characterized by linearly dependent vectors $\vec{\mathbf{N}}$, $\vec{\mathbf{N}}_1$ and $\vec{\mathbf{N}}_2$, where the indices refer again to directional derivatives, cf. (2). In the case of a linear normal field (7), this is only possible for linearly dependent coefficient vectors $\vec{\mathbf{n}}_1$, $\vec{\mathbf{n}}_2$, $\vec{\mathbf{n}}_3$. Thus, if an LN patch has got a parabolic point, then the whole patch consists of parabolic points.

Remark 2. According to our numerical experiences, LN spline surface behave very nicely if the data stem from an elliptic (i.e. locally convex) surface Φ. However, in the case of a hyperbolic surface patch, one has to take a relatively large number of data in order to get reasonable (i.e. regular) results. Also, in this case the shape of the data triangles should be chosen very carefully.

4.4 LN spline surfaces

By composing several macro elements we are able to generate smooth spline surfaces.

Proposition 8 *Consider two Clough–Tocher–type LN macro elements sharing two vertices $\mathbf{v}_1$, $\mathbf{v}_2$ and the associated normals $\vec{\mathbf{m}}_1$, $\vec{\mathbf{m}}_2$. Then, the boundary curve from $\mathbf{v}_1$ to $\mathbf{v}_2$ and the field of normal vectors along the boundary are identical. Consequently, the two macro elements meet with G^1 continuity.*

The proof is straightforward; the boundary curves of both macro elements are identical, as their construction depends solely on the shared data $\mathbf{v}_1$, $\mathbf{v}_2$ and $\vec{\mathbf{m}}_1$, $\vec{\mathbf{m}}_2$. Moreover, due to the LN property, also the normal vectors along the common boundary are identical, hence the patches have a G^1 joint.

In consequence of this observation, the Clough–Tocher–type LN macro elements can be used for generating integral G^1 spline surfaces with rational offsets. An example will be presented in Section 5.4.

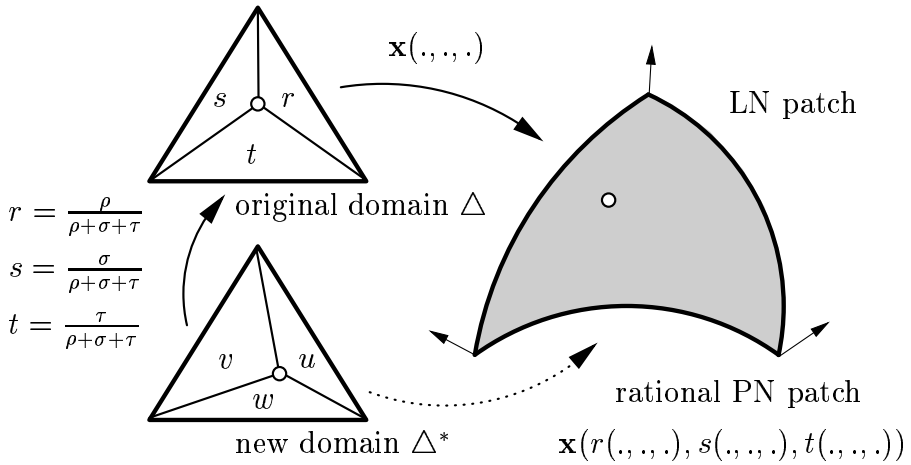

Figure 6: Reparameterization of an LN patch (scheme).

5 Offsetting LN surfaces

Consider an LN patch of degree n with barycentric parameters r, s, t and domain triangle $\triangle$. For instance, it could be one of the three subpatches of the Clough–Tocher–type macro element from Section 4. With the help of a suitable reparameterization we construct an exact rational parameterization of the offset surfaces (10) at a certain distance d. In the sequel, the vertex normals $\vec{\mathbf{n}}_i$ are assumed to be linearly independent, hence the LN patch has no parabolic points.

5.1 Rational representation of the offsets

We introduce new barycentric parameters u, v, w satisfying $u+v+w = 1$ with respect to another domain triangle $\triangle^*$ by substituting

$$r(u,v,w) = \frac{\rho}{\rho+\sigma+\tau},\ s(u,v,w) = \frac{\sigma}{\rho+\sigma+\tau},\ \text{and}\ t(u,v,w) = \frac{\tau}{\rho+\sigma+\tau}, \tag{35}$$

see Figure 6 for a schematic illustration. The bivariate functions $\rho = \rho(u,v,w)$, $\sigma = \sigma(u,v,w)$, and $\tau = \tau(u,v,w)$ are certain bivariate polynomials of degree m in Bernstein–Bézier representation

$$\begin{pmatrix} \rho(u,v,w) \\ \sigma(u,v,w) \\ \tau(u,v,w) \end{pmatrix} = \sum_{\substack{i,j,k \geq 0 \\ i+j+k=m}} B^m_{i,j,k}(u,v,w) \begin{pmatrix} r_{i,j,k} \\ s_{i,j,k} \\ t_{i,j,k} \end{pmatrix} \tag{36}$$

with Bézier coefficients $r_{i,j,k},\ s_{i,j,k},\ t_{i,j,k} \in \mathbb{R}$, respectively. This substitution transforms the squared length of the normal vector into

$$\vec{\mathbf{N}}(r,s,t) \cdot \vec{\mathbf{N}}(r,s,t) = \frac{1}{(\rho+\sigma+\tau)^2} \ \left[\begin{pmatrix} \rho & \sigma & \tau \end{pmatrix} Q \begin{pmatrix} \rho \\ \sigma \\ \tau \end{pmatrix} \right] \tag{37}$$

with the 3×3 Gramian matrix $Q = (q_{i,j})_{i,j=1,2,3} = (\vec{\mathbf{n}}_i \cdot \vec{\mathbf{n}}_j)_{i,j=1,2,3}$ of the vertex normals $\vec{\mathbf{n}}_i$. If the vertex normals $\vec{\mathbf{n}}_i$ are linearly independent, then the Gramian matrix is well–known to be positive definite.

In order to obtain from (10) a *rational* parametric representation of the offsets, we choose the reparameterization such that $\|\vec{\mathbf{N}}(r,s,t)\|$ turns into a (at least piecewise) rational function of the new barycentric parameters u, v, w. According to (37), the bivariate polynomials ρ, σ and τ have to satisfy the identity

$$\begin{pmatrix} \rho(u,v,w) & \sigma(u,v,w) & \tau(u,v,w) \end{pmatrix} Q \begin{pmatrix} \rho(u,v,w) \\ \sigma(u,v,w) \\ \tau(u,v,w) \end{pmatrix} = \xi^2(u,v,w) \tag{38}$$

where

$$\xi(u,v,w) = \sum_{\substack{i,j,k \geq 0 \\ i+j+k=m}} B^m_{i,j,k}(u,v,w)\; x_{i,j,k}. \tag{39}$$

is another polynomial with Bézier coefficients $x_{i,j,k} \in \mathbb{R}$. Consequently, the triangular *rational* Bézier surface

$$\mathbf{y}(u,v,w) = \begin{pmatrix} \rho(u,v,w)/\xi(u,v,w) \\ \sigma(u,v,w)/\xi(u,v,w) \\ \tau(u,v,w)/\xi(u,v,w) \end{pmatrix}, \quad u,v,w \geq 0,\; u+v+w = 1, \tag{40}$$

of degree m with numerator (36) and denominator (39), hence with the homogeneous control points

$$\widetilde{\mathbf{r}}_{i,j,k} = (x_{i,j,k}\; r_{i,j,k}\; s_{i,j,k}\; t_{i,j,k})^\top, \tag{41}$$

describes a triangular patch on the quadric surface

$$\begin{pmatrix} p_1 & p_2 & p_3 \end{pmatrix} Q \begin{pmatrix} p_1 \\ p_2 \\ p_3 \end{pmatrix} = 1 \tag{42}$$

that is generated by the quadratic form associated with the Gramian matrix. If the vertex normals $\vec{\mathbf{n}}_i$ are linearly independent, then this quadratic surface is an *ellipsoid*, due to the positive definiteness of the Gramian matrix. We will refer to it as the *Gramian ellipsoid* associated with the vertex normals. Triangular rational Bézier patches on quadric surfaces have been studied in several publications. More information and many related references can be found in (Sederberg and Anderson 1985) and (Dietz, Hoschek and Jüttler, 1993).

Proposition 9 *Consider a collection of several triangular rational Bézier patches (40) of degree m that describe the first octant of the Gramian ellipsoid (42).* (See

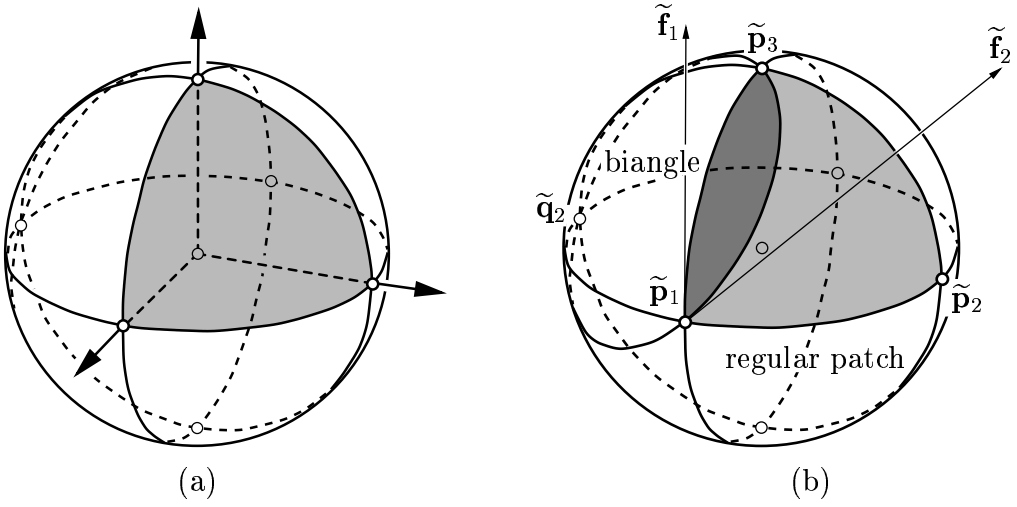

Figure 7: An octant of the Gramian ellipsoid (a) and its quadratic rational parameterization (b).

Figure 7a for an illustration.) *The patches are assumed to have non–negative components ξ, ρ, σ, τ for its domains Δ^*, i.e. for barycentric parameters $u, v, w \geq 0$, $u+v+w=1$. The denominator ξ is even assumed to be strictly positive. Then, the reparameterization (35) produces an exact representation of the offset surface (10) by rational Bézier surface patches of degree $m(n+1)$, where n is the degree of the LN patch.*

Proof. Assume that the first octant of the Gramian ellipsoid has been parameterized as described in the proposition. Consider a point $\mathbf{x}(r,s,t)$ on the LN surface patch. The ray $(\lambda r \;\; \lambda s \;\; \lambda t)^\top$, $\lambda \in \mathbb{R}_+$, intersects one of the patches covering the first octant of the Gramian ellipsoid at a certain point

$$(\rho(u_0,v_0,w_0)/\xi(u_0,v_0,w_0) \;\; \sigma(\ldots)/\xi(\ldots) \;\; \tau(\ldots)/\xi(\ldots))^\top. \tag{43}$$

Consequently, as the numerator ξ was assumed to be positive, the substitution (35) reproduces the original barycentric parameters (r,s,t), hence the original surface point.

Owing to (37) and with the help of the identity (38) we get

$$\sqrt{\vec{\mathbf{N}} \cdot \vec{\mathbf{N}}} = \frac{\xi}{\rho+\sigma+\tau}. \tag{44}$$

For each patch on the Gramian ellipsoid, the parametric representation (10) of the offset at distance d leads to

$$\mathbf{x}_d = \frac{\mathbf{x}(\rho,\sigma,\tau)}{(\rho+\sigma+\tau)^n} + d\,\frac{\rho+\sigma+\tau}{\xi}\,\frac{N(\rho,\sigma,\tau)}{\rho+\sigma+\tau} = \frac{\xi\,\mathbf{x}(\rho,\sigma,\tau) + d\,(\rho+\sigma+\tau)^n\,N(\rho,\sigma,\tau)}{\xi\,(\rho+\sigma+\tau)^n}. \tag{45}$$

The common denominator $\rho+\sigma+\tau$ of the substitution (35) produces the denominators of the LN patch $\mathbf{x}$ and of the normals $\vec{\mathbf{N}}$, as both expressions are homogeneous polynomials of the barycentric parameters r, s, t. By generating the Bernstein–Bézier representation of (45) we obtain a triangular rational Bézier patch of degree $m(n+1)$ with respect to the barycentric parameters u, v, w. □

Thus, with the help of a rational parameterization of the associated Gramian ellipsoid, a given LN patch can be transformed into a Pythagorean normal surface.

Remark. For the offset at distance 0 (i.e. the original surface), the degree of the reparameterized surface (45) reduces to mn, as the second term vanishes.

5.2 Parameterizing the Gramian ellipsoid

In order to represent the offset surfaces $\mathbf{x}_d(r, s, t)$ by rational Bézier patches of minimum degree, the degree of the patches covering the octant of the ellipsoid should be kept as low as possible. Consequently, we will parameterize the Gramian ellipsoid by quadratic rational patches. However, there is the following negative result.

Lemma 10 *In general, the first octant of the Gramian ellipsoid cannot be parameterized by a collection of regular rational quadratic Bézier triangles.*

Proof. With the help of a suitable affine transformation, the Gramian ellipsoid can be mapped into a sphere. The octant is then transformed into a spherical triangle that is bounded by segments of circular arcs. According to the results on regular quadratic Bézier triangles on spheres, the sum of the interior angles equals π, as the three boundary circles always intersect in one point, see Boehm and Hansford (1991), Dietz, Hoschek and Jüttler (1993), or Sederberg and Anderson (1985). Consequently, if a collection of regular quadratic Bézier triangles covers a segment of the sphere, then the interior angles of this segment sum up to a multiple of π. In general, however, the interior angles of the octant's image under the affine transformation are not a multiple of π. For instance, if the Gramian ellipsoid is a sphere itself (this is the case for mutually perpendicular vertex normals $\vec{\mathbf{n}}_i$ of uniform length), then the interior angles of the octant of a sphere sum up to $3/2\pi$. This proves the result. □

We decompose the first octant of the Gramian ellipsoid into two quadratic triangular Bézier patches, see Figure 7b. One of the two patches describes a *biangle*, as one of its boundaries degenerates into a point. The homogeneous control points of the patches have been gathered in equations (50) and (53). Readers who are not interested in the details of the construction may skip the explanations below.

Both patches are constructed with the help of stereographic projection, cf. (Geise and Langbecker, 1990). In order to keep the notation as simple as possible we shall

use homogeneous coordinates $\widetilde{\mathbf{p}} = (\widetilde{p}_0 \dots \widetilde{p}_4)^\top \in \mathbb{R}^4 \setminus \{(0\ 0\ 0\ 0)^\top\}$. The standard Cartesian coordinates $\mathbf{p} = (p_1\ p_2\ p_3)^\top$ of points are obtained from $p_i = \widetilde{p}_i/\widetilde{p}_0$, $\widetilde{p}_0 \neq 0$. Linearly dependent vectors of homogeneous coordinates correspond to the same point. Homogeneous coordinates with $\widetilde{p}_0 = 0$ correspond to points at infinity; they can be seen as the intersection of parallel lines with direction $(\widetilde{p}_1\ \widetilde{p}_2\ \widetilde{p}_3)^\top$. For more information on homogeneous coordinates, the reader should consult any textbook on projective geometry.

Using homogeneous coordinates, the equation of the Gramian ellipsoid (42) transforms into $\widetilde{\mathbf{p}}^\top \widetilde{Q}\, \widetilde{\mathbf{p}} = 0$, with the real symmetric 4×4–matrix

$$\widetilde{Q} = \left(\begin{array}{c|ccc} -1 & 0 & 0 & 0 \\ \hline 0 & & & \\ 0 & & Q & \\ 0 & & & \end{array}\right) \tag{46}$$

Consider a point $\widetilde{\mathbf{c}}$ on the Gramian ellipsoid. The mapping

$$\widetilde{\mathbf{x}} \mapsto (\widetilde{\mathbf{x}}^\top \widetilde{Q}\, \widetilde{\mathbf{x}})\, \widetilde{\mathbf{c}} - 2(\widetilde{\mathbf{c}}^\top \widetilde{Q}\, \widetilde{\mathbf{x}})\, \widetilde{\mathbf{x}} \tag{47}$$

maps any point $\widetilde{\mathbf{x}}$ to the intersection of the line $\widetilde{\mathbf{p}} \vee \widetilde{\mathbf{c}}$ with the Gramian ellipsoid, see (Geise and Langbecker, 1990). This mapping will be called the *stereographic projection with centre* $\widetilde{\mathbf{c}}$.

Recall that Gramian matrix of the vertex normals has the components $q_{i,j} = \vec{\mathbf{n}}_i \cdot \vec{\mathbf{n}}_j$, and let $n_i = \|\vec{\mathbf{n}}_i\| = \sqrt{q_{i,i}}$. We compute the intersections of the coordinate axes with the Gramian ellipsoid,

$$\begin{array}{ll} \widetilde{\mathbf{p}}_1 = (1\ 1/n_1\ 0\ 0)^\top, & \widetilde{\mathbf{p}}_2 = (1\ 0\ 1/n_2\ 0)^\top, \\ \widetilde{\mathbf{p}}_3 = (1\ 0\ 0\ 1/n_3)^\top, & \widetilde{\mathbf{q}}_2 = (1\ 0\ -1/n_2\ 0)^\top, \end{array} \tag{48}$$

see Figure 7b. In order to construct the regular quadratic patch, we apply the stereographic projection with centre $\widetilde{\mathbf{q}}_2$ to the rational linear Bézier patch

$$\widetilde{\mathbf{x}}^{(t)}(u,v,w) = u\, \widetilde{\mathbf{p}}_1 + v/2\, \widetilde{\mathbf{p}}_2 + w\, \widetilde{\mathbf{p}}_3 \tag{49}$$

with vertices (control points) $\widetilde{\mathbf{p}}_i$. The factor $1/2$ at $\widetilde{\mathbf{p}}_2$ is introduced in order to simplify the result. The stereographic projection (47) with $\widetilde{\mathbf{c}} = \widetilde{\mathbf{q}}_2$ produces the quadratic rational Bézier patch $\mathbf{y}^{(t)}(u,v,w)$ (see (40)) with the homogeneous control points

$$\begin{array}{l} \widetilde{\mathbf{r}}^{(t)}_{2,0,0} = \frac{2\,n_1 n_2 + 2\,q_{1,2}}{n_1 n_2}\, \widetilde{\mathbf{p}}_1, \quad \widetilde{\mathbf{r}}^{(t)}_{1,1,0} = (1 + \frac{q_{1,2}}{n_1 n_2}\ \ \frac{1}{n_1}\ \ \frac{1}{n_2}\ 0)^\top, \\ \widetilde{\mathbf{r}}^{(t)}_{1,0,1} = \frac{1}{n_1 n_2 n_3}\, (n_2 n_3 n_1 + q_{1,3} n_2 + q_{1,2} n_3 + q_{2,3} n_1\ \ n_2 n_3 + q_{2,3}\ \ n_1 n_3 - q_{1,3}\ \ n_1 n_2 + q_{1,2})^\top, \\ \widetilde{\mathbf{r}}^{(t)}_{0,2,0} = \widetilde{\mathbf{p}}_2, \quad \widetilde{\mathbf{r}}^{(t)}_{0,1,1} = (1 + \frac{q_{2,3}}{n_2 n_3}\ \ 0\ \ \frac{1}{n_2}\ \ \frac{1}{n_3})^\top, \quad \widetilde{\mathbf{r}}^{(t)}_{0,0,2} = 2\,(1 + \frac{q_{2,3}}{n_2 n_3})\, \widetilde{\mathbf{p}}_3, \end{array} \tag{50}$$

cf. (41). In order to find the analogous representation of the biangle patch, we introduce two points $\widetilde{\mathbf{f}}_1$, $\widetilde{\mathbf{f}}_2$ at infinity,

$$\begin{aligned}\widetilde{\mathbf{f}}_1 &= (0 \;\; -q_{1,3} \;\; 0 \;\; n_1^2)^\top \quad \text{and} \\ \widetilde{\mathbf{f}}_2 &= (0 \;\; -q_{1,3}n_2 - q_{1,2}n_3 \;\; n_1(n_1n_3 - q_{1,3}) \;\; n_1(n_1n_2 + q_{1,2}))^\top.\end{aligned} \tag{51}$$

Both points are infinite points of tangents to the Gramian ellipsoid at $\widetilde{\mathbf{p}}_1$. The first (resp. second) point belongs to the tangent that is contained in the plane spanned by the origin, $\widetilde{\mathbf{p}}_1$ and $\widetilde{\mathbf{p}}_3$ (resp. by $\widetilde{\mathbf{p}}_1$, $\widetilde{\mathbf{p}}_3$ and $\widetilde{\mathbf{q}}_2$). Note that $\widetilde{f}_{1,3} > 0$, $\widetilde{f}_{2,2} > 0$ and $\widetilde{f}_{2,3} > 0$, hence the orientation of the associated direction vectors is as indicated by the arrows in Figure 7b.

The quadratic rational representation $\mathbf{y}^{(b)}(u,v,w)$ of the biangle is obtained by applying the stereographic projection with centre $\widetilde{\mathbf{c}} = \widetilde{\mathbf{p}}_1$ to the rational linear Bézier patch

$$\widetilde{\mathbf{x}}^{(b)}(u,v,w) = u/n_1\,\widetilde{\mathbf{f}}_2 + v/n_1\,\widetilde{\mathbf{f}}_1 + w\,\widetilde{\mathbf{p}}_3. \tag{52}$$

Again, the factors $1/n_1$ at $\widetilde{\mathbf{f}}_i$ are introduced in order to simplify the result. The homogeneous control points of the biangle patch are

$$\begin{aligned}&\widetilde{\mathbf{r}}^{(b)}_{2,0,0} = 2\,(n_1n_2+q_{1,2})(n_2n_3+q_{2,3})\,\widetilde{\mathbf{p}}_1, \;\; \widetilde{\mathbf{r}}^{(b)}_{1,1,0} = (n_2n_3n_1+q_{1,3}n_2+q_{1,2}n_3+q_{2,3}n_1)\,\widetilde{\mathbf{p}}_1, \\ &\widetilde{\mathbf{r}}^{(b)}_{1,0,1} = n_2\,\widetilde{\mathbf{r}}^{(t)}_{1,0,1}, \;\; \widetilde{\mathbf{r}}^{(b)}_{0,2,0} = (n_1n_3+q_{1,3})\,\widetilde{\mathbf{p}}_1, \;\; \widetilde{\mathbf{r}}^{(b)}_{0,1,1} = (1+\tfrac{q_{1,3}}{n_1n_3} \;\; \tfrac{1}{n_1} \;\; 0 \;\; \tfrac{1}{n_3})^\top, \;\; \widetilde{\mathbf{r}}^{(b)}_{0,0,2} = \tfrac{2}{n_1n_3}\widetilde{\mathbf{p}}_3.\end{aligned} \tag{53}$$

In order to improve the distribution of the parametric speed on the offset surfaces, the two quadratic patches (50), (53) should be brought into *standard form* (Farin, 1995) by transforming the control points according to

$$\widetilde{\mathbf{r}}^{(l)}_{i,j,k} \mapsto \lambda^j\,\mu^k\,\widetilde{\mathbf{r}}^{(l)}_{i,j,k} \;\text{ with }\; \lambda = \sqrt{r^{(l)}_{2,0,0|0}/r^{(l)}_{0,2,0|0}}, \quad \mu = \sqrt{r^{(l)}_{2,0,0|0}/r^{(l)}_{0,0,2|0}}, \;\; l \in \{t,b\}, \tag{54}$$

where the indices $_{|0}$ refer to the weight (0th) component of the homogeneous coordinates. This operation produces identical weights at the three vertices; it corresponds to a bilinear transformation of the barycentric parameters u, v, w.

An example is shown in Figure 8. The Gramian ellipsoid has been obtained from the vertex normals $(2,0,-0.6)^\top$, $(-0.1,3,0)^\top$ and $(0,0,5)^\top$; its principal axes are not the axes of the coordinate system. The figure shows the control points $\widetilde{\mathbf{r}}^{(l)}_{i,j,k}$ of the two quadratic rational patches. Clearly, the control points along the inner boundary (shown as dashed curve) are identical.

5.3 Generating the offsets

With the help of the quadratic patches $\mathbf{y}^{(l)}(u,v,w)$ covering the first octant of the Gramian ellipsoid, it is now possible to generate exact rational Bézier representations

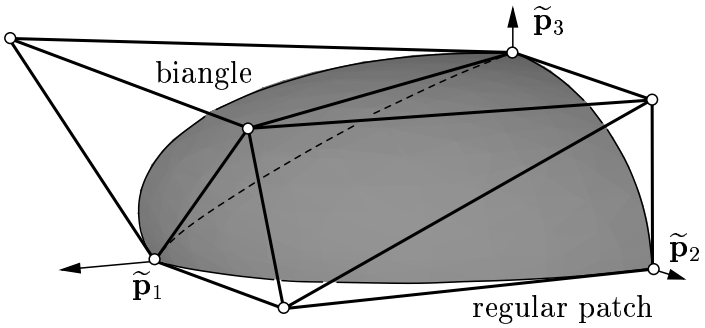

Figure 8: The quadratic patches on a Gramian ellipsoid.

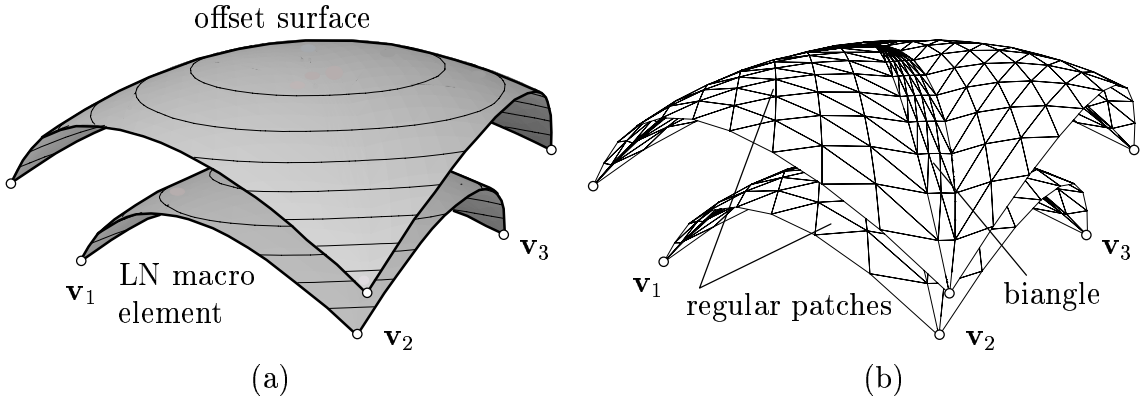

Figure 9: LN macro element and offset surface for convex data (a) and the control nets (b).

of LN patches, according to Proposition 9. The offset surface of an LN surface is then described by two rational Bézier triangles of degree $2(n+1)$, see (45). In the case of the subpatches of the LN macro element, we obtain two rational patches of degree 10, each having $\binom{12}{2} = 66$ Bézier control points. In order to compute these control points, one has to evaluate certain compositions of Bernstein polynomials, e.g. $\mathbf{x}(\rho(u,v,w), \sigma(\ldots), \tau(\ldots))$. Suitable algorithms for these computations have been developed by DeRose (1988).

As an example, Figure 9a shows an LN macro element and its offset. The LN macro element matches three G^1 data $(\mathbf{v}_i, \vec{\mathbf{m}}_i)$ that are taken from a convex surface. In addition to the macro element, the figure shows the offset surface at a certain distance d; it is described by 6 rational Bézier triangles of degree 10 which are obtained after the quadratic rational reparameterization. Both the original surface and its offset are visualized by level curves, i.e., by intersections with a system of parallel planes.

The quadratic reparameterization has been applied to the LN macro element also, producing 6 rational Bézier triangles of degree $2n = 8$, cf. (45). The Bézier control

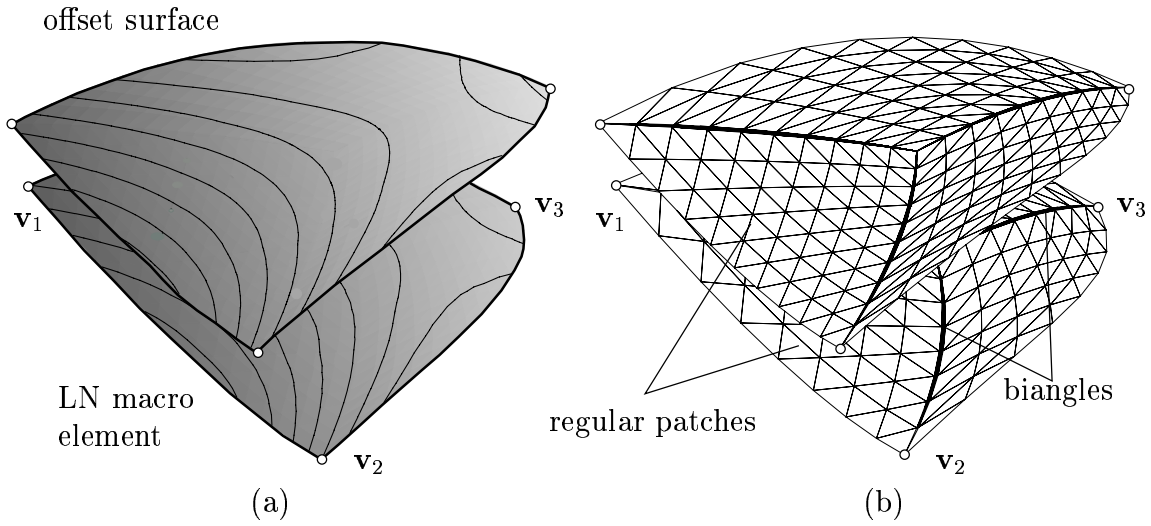

Figure 10: LN macro element and offset surface for non–convex data (a) and the control nets (b).

nets, along with the given vertex data, have been drawn in figure 9b. The biangle patch on the Gramian ellipsoid produces degenerate rational Bézier triangles, where one boundary curve collapses into one point.

Similarly, Figure 10 shows an LN macro element and its offset that are obtained from non–convex data (a) and the associated Bézier control nets (b). Here, the biangle patches are relatively long and thin; this happens if the boundary normals $\vec{\mathbf{m}}_i$ are almost parallel. Thus, in this situation it might be more appropriate to use an alternative representation of the Gramian octant, see the remark below.

Remark. Using degenerate Bézier triangles may entail problems in applications. In our situation, there are two possibilities to circumvent the problem of degenerate representations.

- On one hand, the octant of the Gramian ellipsoid could be parameterized by triangular Bézier surfaces of *degree 4*. Using such patches it is possible to describe the octant as a single rational Bézier surface, see (Joe and Wang, 1994) for more details. However, as a disadvantage of this approach, the degree of the offsets $(4n + 4)$ becomes relatively high; it would be 20 for the subpatches of the LN macro element, producing patches with $\binom{22}{2} = 231$ control points.

- Alternatively one might use quadratic triangular patches with a generalized parameter domain, so–called *trimmed patches*. For instance, the domain Δ^* of the regular quadratic patch $\mathbf{y}^{(t)}(u, v, w)$ could be extended, in oder to describe the whole octant of the ellipsoid. This produces a triangular region in the parameter domain, where one of the boundaries is a certain conic section. Using this

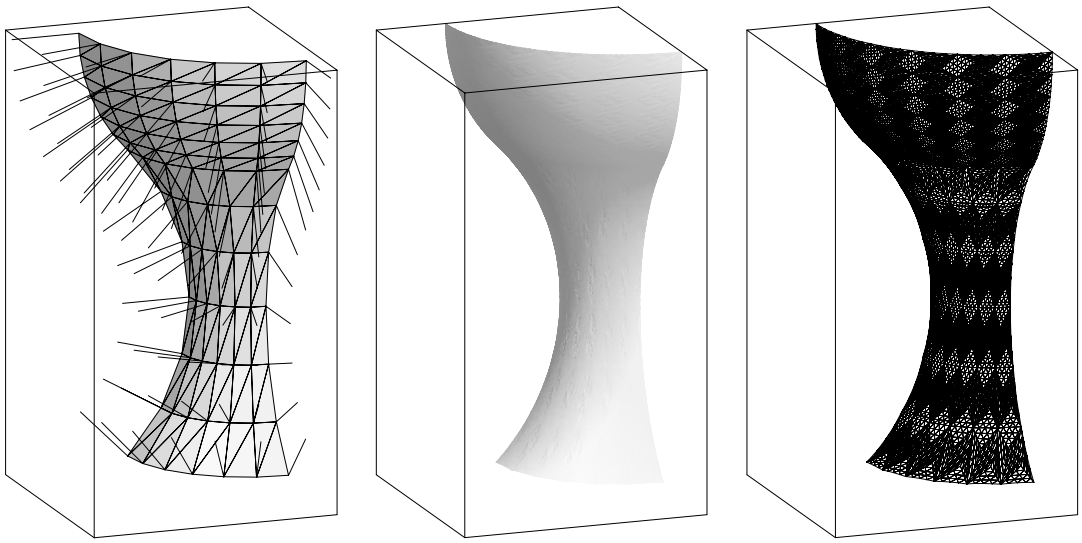

Figure 11: LN spline surface describing a quarter of a glass–shaped object. The data (a), the LN spline surface (b) and the Bézier control net (c).

approach, the offsets can be represented as trimmed triangular Bézier patches of degree 10. Similarly it is possible to derive trimmed tensor–product representations of degree $(10, 10)$. These representations may be most useful in applications, as trimmed tensor–product patches are supported by the current CAD data exchange standards, such as IGES or STEP.

5.4 Offsets of LN spline surfaces – an example

Figure 11 shows an example, modeling a quarter of a glass–shaped object. The data (triangulated points with associated normals, see Figure 11a) have been sampled from a surface of revolution whose meridian consists of two circular arcs. Consequently, the original surface is composed of two toroidal patches. Note that the original surface has no parabolic points as it is not C^2 along the common boundary of the toroidal patches. The triangulated data points are interpolated by a LN spline surface of degree 4, see Figure 11b,c. Note that any affine image of the LN spline surface is again a LN spline surface, as the class of surfaces with linear normals is affinely invariant, see (Jüttler 1998).

The offset of the LN spline surface at a certain distance d can be represented exactly by rational Bézier triangles of degree 10. Figure 12 shows the offset surface of a surface strip (not covering the whole of the quarter). The figure has been

generated with the help of the exact rational Bézier representation, as described in the previous section.

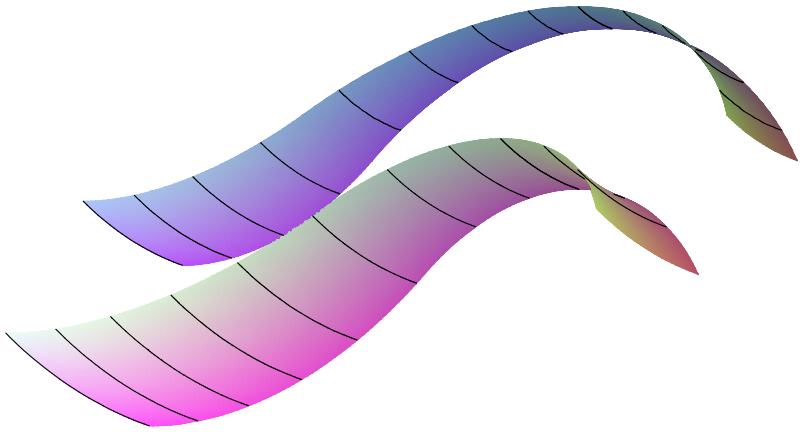

Figure 12: A surface strip of the LN spline surface and its offset.

5.5 Surface conversion vs. offset approximation

The construction described in this paper can be used for approximately converting any given surface (without parabolic points) into an integral spline surface with rational offsets. Clearly, in many applications, it will be more appropriate to use the traditional methods for offset surface approximation, as they deal directly with the offset, rather than with the base surface. However, if the initial surface is not given in a standard CAD representation (e.g., in reverse engineering), then the conversion into LN form might be a useful approach, too.

As an advantage, the LN surface spline scheme reproduces the singularities (edges and self–intersections) of the offset surfaces very well, without any need for additional segmentations. Traditional schemes for offset surface approximation, by contrast, will have difficulties with these singularities. An example is given in Figure 13a, showing an octant of the ellipsoid with the diameters $(7, 10, 15)$, along with its inner offset at distance 6.5. The singularities of the offset are clearly visible. The surface patch has been approximated by 3 LN macro elements. The control nets of the LN spline surface and of its offset have been drawn in Figure 13b. The shaded images of the approximating surfaces have not been drawn, as they are virtually identical to the plot (a) of the original surfaces.

Alternatively, the construction described in this paper can also be used for interpolating given point data with a LN spline surface. If the associated normal vectors are not yet known, then they have to be estimated from the data. There are various possibilities to generate suitable estimates, e.g., with the help of auxiliary surfaces

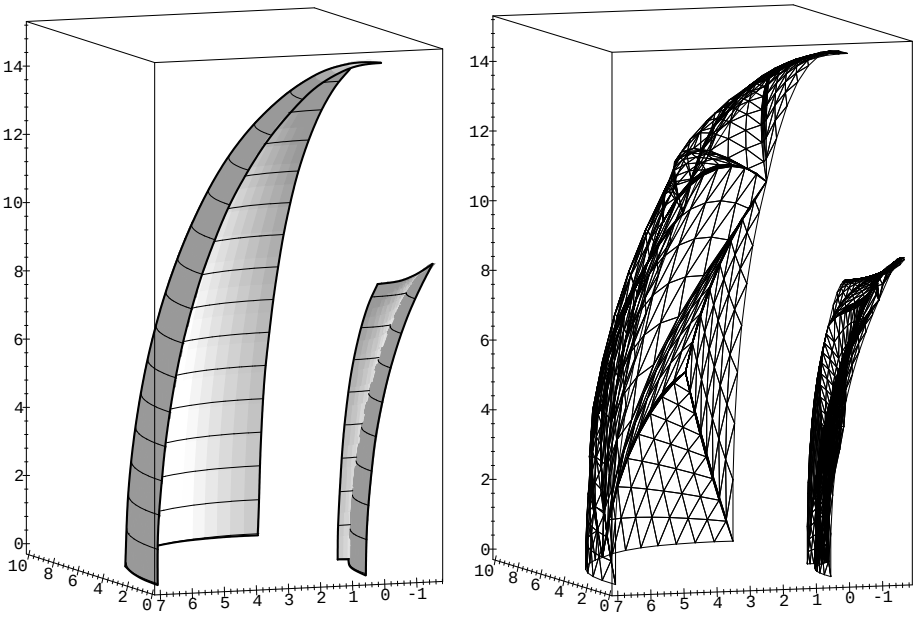

(a) (b)

Figure 13: Inner offset of an ellipsoid. The original surfaces (a) and the control nets of the LN spline approximation (b).

which are locally fitted to the data. These auxiliary surface may then also be used for generating additional vertices, if required.

6 Conclusion

As demonstrated in this paper, using Clough–Tocher–type LN macro elements it is possible to generate integral spline surfaces with rational offsets. The offset surfaces can be described by rational triangular Bézier patches of degree 10, however requiring degenerate patches (biangles). Alternatively, in order to avoid the degenerate vertices, one may use trimmed surface representations, e.g. trimmed tensor–product patches of degree 10, or regular triangular patches of degree 20.

Unlike the dual approach to PN surfaces, we have used the defining property of a linear normal vector field as a linear constraint on the space of integral patches. Consequently, we obtain an integral spline surface that is embedded into a family of rational offsets. This approach facilitates the construction of surface patches which are free of singularities, such as cusps and points at infinity.

Further research may focus on the following questions. Firstly, the construction of cubic LN spline surface of minimum polynomial degree might be of some interest, as this will help to obtain offset surfaces of lower degree, without need for singular

parameterization. Secondly, we will try to generalize the result of theorem 6 concerning the regularity of the boundaries to the LN patches themselves. This might be possible by using more sophisticated techniques for dealing with the resulting linear system of equations.

Acknowledgement

The second author was working on this project while she was visiting the University of Technology, Darmstadt. The financial support of this visit by a postdoctoral research grant of the *Consiglio Nazionale delle Ricerche* of Italy, and the hospitality of her host, Professor J. Hoschek at Darmstadt, are gratefully acknowledged.

The authors wish to thank the anonymous referees for their reports which have helped to improve the manuscript.

References

Barnhill, R.E. and Frost, T.M. (1995), Parametric offset surface approximation, in: Hagen, H. et al., eds., *Geometric modelling*, Comput. Suppl. 10, 1–34. Springer, Vienna.

Boehm, W. and Hansford, D. (1991), Bézier patches on quadrics, in: Farin, G.E., ed., *NURBS for curve and surface design*, SIAM, Philadelphia, 1–14.

Clough, R.W. and Tocher, J.L. (1965), Finite element stiffness matrices for the analysis of plate bending, in: *Proc. of the 1st Conference on Matrix Methods in Structural Mechanics*, Wright-Patterson AFB AFFDL TR 66-80, 515–545.

DeRose, T.D. (1988), Composing Bézier simplexes, ACM Transactions on Graphics 7, 198–221.

Dietz, R., Hoschek, J. and Jüttler, B. (1993), An algebraic approach to curves and surfaces on the sphere and on other quadrics, Comput. Aided Geom. Design 10, 211–229.

Elber, G. and Cohen, E. (1991), Error bound variable distance offset operator for free form curves and surfaces, Int. J. of Comp. Geom. & Appl. 1, 67–78.

Elber, G., Lee, I.-K. and Kim, M.-S. (1997), Comparing Offset Curve approximation methods, IEEE Computer Graphics and Applications 17.3, 62–71.

Farin, G.E. (1986), Triangular Bernstein-Bézier patches, Comput. Aided Geom. Design 3, 83–127.

Farin, G.E. (1995), *NURB curves and surfaces*, AK Peters, Wellesley (Mass.).

Farouki, R.T. (1986), The approximation of non-degenerate offset surfaces, Comput. Aided Geom. Design 3, 15–43.

Farouki, R.T. (1994), The conformal map $z \to z^2$ of the hodograph plane, Comput. Aided Geom. Design 11, 363–390.

Farouki, R.T. and Neff, C.A. (1995), Hermite interpolation by Pythagorean hodograph quintics, Math. Comput. 64, 1589–1609.

Farouki, R.T. and Pottmann, H. (1996), Polynomial and rational Pythagorean-hodograph curves reconciled, in: Mullineux, G., ed., *The Mathematics of Surfaces VI*, Oxford University Press, 355–378.

Farouki, R.T. and Sederberg, T.W. (1995), Analysis of the offset to a parabola, Comput. Aided Geom. Design 12, 639–645.

Fiorot, J.C. and Gensane, Th. (1994), Characterizations of the set of rational parametric curves with rational offsets, in: Laurent, P.-J. et al., eds., *Curves and surfaces in geometric design*, AK Peters, Wellesley, 153–160 (1994).

Geise, G. and Langbecker, U. (1990), Finite quadric segments with four conic boundary curves, Comput. Aided Geom. Design 7, 141–150.

Hoschek, J. and Lasser, D. (1993), *Fundamentals of Computer Aided Geometric Design,* AK Peters, Wellesley (Mass.).

Hoschek, J., Schneider, F.-J. and Wassum, P. (1989), Optimal approximate conversion of spline surfaces, Comput. Aided Geom. Design 6, 293–306.

Joe, B. and Wang, W. (1994), Reparameterization of rational triangular Bezier surfaces, Comput. Aided Geom. Design 11, 345–361.

Jüttler, B. (1998), Triangular Bézier surface patches with a linear normal vector field, in: Cripps, R., ed., *The Mathematics of Surfaces VIII*, Information Geometers, Winchester, 431–446.

Kolb, A., Pottmann, H. and Seidel, H.-P. (1995), Surface reconstruction based upon minimum norm networks, in: Dæhlen, M. et al., eds., *Mathematical methods for curves and surfaces*, Vanderbilt University Press, Nashville, 292–304.

Patrikalakis, N.M. and Prakash, V. (1987) Free-form plate modeling using offset surfaces, in: Chung, J.S. and Angelides, D., eds, *Computers in offshore and arctic engineering*, ASME, New York, 37–44.

Peternell, M. (1997), *Rational Parametrizations for Envelopes of Quadric Families*, Ph.D. thesis, Institute of Geometry, University of Technology, Vienna.

Peternell, M. and Pottmann, H. (1996), Designing rational surfaces with rational offsets, in: Fontanella, F. et al., eds., *Advanced Topics in Multivariate Approximation*, World Scientific, Singapore, 275–286.

Pottmann, H. (1995), Rational curves and surfaces with rational offsets, Comput. Aided Geom. Design 12, 175–192.

Sabin, M.A. (1974), A Class of Surfaces closed under five important geometric operators, Report VTO/MS/207, British Aircraft Corporation Ltd., Commercial Aircraft Division, Weybridge; retypeset and footnotes added 1999, available from M.A. Sabin's homepage at `http://www.damtp.cam.ac.uk`.

Sederberg, T. and Anderson, D. (1985), Steiner surface patches, IEEE Comput. Graphics Appl. 5, 23–36.